

Collisional mechanism for GRB emission

Andrei M. Beloborodov^{*}

*Physics Department and Columbia Astrophysics Laboratory, Columbia University, 538 West 120th Street New York, NY 10027;
amb@phys.columbia.edu*

18 April 2019

ABSTRACT

GRB jets are expected to carry a neutron component. Strong collisional heating operates in such jets. It is shown to produce bright emission with a spectrum consistent with observations. The radiative mechanism involves inelastic collisions between neutrons and protons, which create multiple e^\pm with energies $\sim m_\pi c^2 \approx 140$ MeV. The created e^\pm quickly radiate their energy and thermalize. The thermalized e^\pm population is heated by Coulomb collisions with protons. Numerical simulations of collisionally heated jets are presented. The simulations track the evolution of e^\pm plasma and radiative transfer in the expanding jet. Jets with Lorentz factors $\Gamma \gtrsim 500$ produce the photon spectrum that peaks near 1 MeV and extends to GeV energies with a slope of 2.3–2.5, which is the typical spectrum reported by GRB observations. Most of this radiation is emitted near the photosphere of the jet. The sub-photospheric collisional heating converts $\gtrsim 30$ per cent of the explosion energy to escaping radiation. Additional emission is expected at later stages when neutrons decay and produce collisionless heating.

Key words: gamma-rays: bursts, theory — plasmas — radiation mechanisms: thermal, nonthermal — radiative transfer — relativity — scattering.

1 INTRODUCTION

Gamma-ray bursts (GRBs) are associated with ultra-relativistic jets from short-lived powerful sources such as hyper-accreting, just born black holes. The jet starts as a blackbody fireball that accelerates, expands and releases its radiation. However, the simple blackbody emission model is inconsistent with observations (e.g. Piran 2005). It is clear that some form of heating operates in the jet and changes its radiation from blackbody. Two heating models are usually considered: internal shocks and dissipation of magnetic energy. Both mechanisms are essentially *collisionless* and rely on collective plasma processes in the jet that are not completely understood. A long-standing problem is the radiative efficiency of these processes. In particular, it remains unclear what fraction of energy dissipated in internal shocks is given to electrons and eventually to radiation. Advanced plasma simulations show no electron acceleration in magnetized transverse shocks that are usually assumed in GRB jets (Sironi & Spitkovsky 2009).

The present paper proposes a different mechanism that relies only on *collisional* processes, which are well understood. Previous work on nuclear collisions in GRB jets showed that the collisions become rare before the

jet expands to transparency (Derishev, Kocharovsky & Kocharovsky 1999). This has two reasons: (1) the cross section for nuclear collisions is small, $\sim 1/20$ of the photon scattering cross section, and (2) creation of e^\pm pairs increases the optical depth of the jet and delays its transparency to radiation. Nuclear collisions were previously investigated mainly as a source of e^\pm and neutrinos, which easily escape the opaque flow. In particular, the presence of a free neutron component leads to significant emission of multi-GeV neutrinos (Derishev et al. 1999; Bahcall & Mészáros 2000; Mészáros & Rees 2000). This prediction may be verified by future neutrino detectors. The existing upper limits from Super-Kamiokande experiment are ~ 10 times above the expected neutrino flux (Fukuda et al. 2002).

The main result of the present paper is that collisional processes in baryonic jets generate photospheric γ -ray emission with the observed spectrum from ~ 10 keV to \sim GeV. Neutrons play a key role for this emission. Neutron-loaded jets develop ‘compound’ flows: a plasma with bulk Lorentz factor Γ embedding a neutron flow with Lorentz factor $\Gamma_n \ll \Gamma$ (Derishev et al. 1999; Mészáros & Rees 2000). Nuclear collisions in the compound flow dissipate and re-dissipate energy that can exceed the total energy of the flow. A significant fraction of the dissipated energy is given to created e^\pm and immediately converted to radiation, which greatly increases the radiative efficiency of the GRB. Similarly to internal shocks, the collisional mechanism taps the

^{*} Also at Astro-Space Center of Lebedev Physical Institute, Profsojuznaja 84/32, Moscow 117810, Russia

kinetic energy of internal motions in the jet, in particular the streaming of plasma through the neutron component with a relative Lorentz factor $\Gamma_{\text{rel}} > 1$. In contrast to internal shocks, the heating is not confined to a shock front. Instead, it operates in volume.

The collisional heating can be classified as so-called ‘slow heating,’ which contrasts with quick particle acceleration in shocks. Perhaps a better name would be ‘volume heating’ as it occurs in volume rather than is localized to a shock front. Several works previously proposed volume heating as a source of GRB radiation (e.g. Thompson 1994; Ghisellini & Celotti 1999; Stern & Poutanen 2004; Rees & Mészáros 2005; Pe’er, Mészáros & Rees 2005; Giannios & Spruit 2007). The models assumed collisionless dissipation, which is difficult to calculate. In this context, two special features of the proposed mechanism should be noted:

(i) The collisional heating is robust. Its history in the expanding jet is well defined. The rate of collisions determines the radial dependence of the heating rate $\dot{Q} \propto r^{-2}$.

(ii) The collisional heating occurs via two branches with comparable heating rates:

(a) Nuclear collisions maintain a continual nonthermal e^\pm cascade.

(b) Coulomb collisions in the two-temperature plasma¹ continually transfer energy from protons to thermalized e^\pm .

Branch (a) is important because it loads the jet with a large number of e^\pm pairs and determines the photosphere radius (Derishev et al. 1999). On the other hand, it will be shown that branch (b) plays a key role in the formation of the GRB spectrum. Radiation emerging from a collisionally heated jet has a well defined spectrum, which can be calculated numerically. This radiative transfer problem is solved in this paper using a Monte-Carlo code that tracks the evolution of photons and e^\pm in the heated and expanding plasma flow.

Section 2 gives a compact summary of the standard ‘fireball’ model of GRBs, with no neutrons and no variability. Such jets passively cool down as they expand, and eventually emit thermal radiation whose spectrum cuts off exponentially at \lesssim MeV. It is inconsistent with the observed nonthermal spectrum that extends to GeV energies. We use the model of a passively cooling jet as a benchmark and a first simplest test for the radiative transfer code.

Section 3 describes neutron-loaded jets and formation of compound flows with $\Gamma_n < \Gamma$. Section 4 describes the collisional radiative mechanism operating in compound flows. Section 5 presents the radiation spectrum emitted to distant observers. The results are discussed in Section 6.

GRB outflows are likely to be beamed and therefore called ‘jets’ throughout this paper. However, the results apply equally well to spherically symmetric outflows. As long as the opening angle of the explosion is larger than $1/\Gamma$, the jet near the axis is causally disconnected from its edge, and its dynamics is the same as that of a spherically symmetric flow.

¹ The thermalized e^\pm are Compton-cooled and kept at a temperature much lower than the proton temperature.

2 THERMAL EMISSION FROM PASSIVELY COOLING JETS

We focus in this paper on jets that are accelerated by thermal (radiation) pressure, with a subdominant magnetic field. This standard model is briefly summarized below (see e.g. Paczyński 1990).

At small radii r , the GRB jet is in thermodynamic equilibrium and its luminosity is carried mainly by radiation $L \approx (4/3)caT^4\Gamma^2 4\pi r^2$ (hereafter we use the isotropic equivalent of luminosity, which would be produced by a spherically symmetric outflow of the same density and temperature). As the jet expands adiabatically, the ratio of photon and baryon number densities n_γ/n remains constant, i.e. effectively the photon number is conserved (similar to the big bang). The jet accelerates until the radiation energy density $U_\gamma = aT^4$ decreases below the rest-mass density $nm_p c^2$. Then its Lorentz factor saturates at the asymptotic Γ . We will denote the characteristic saturation radius by R_s . For a radially expanding jet,

$$R_s \approx \Gamma r_0, \quad (1)$$

where r_0 is the radius at the base of the jet, at the beginning of its acceleration. For collimated jets, the effective r_0 can be significantly larger than the central engine. The photon-to-baryon ratio in the jet is given by

$$\frac{n_\gamma}{n} \approx 240 \Gamma r_{0,7}^{1/2} L_{52}^{-1/4}, \quad (2)$$

and the jet energy *per photon* is

$$\bar{E}_0 \approx \frac{\Gamma m_p c^2 n}{n_\gamma} \approx 4 r_{0,7}^{-1/2} L_{52}^{1/4} \text{ MeV}. \quad (3)$$

If no heat is generated by any dissipation processes, the thermal radiation trapped in the opaque flow continues to cool adiabatically at $r > R_s$ until it is released at the photosphere R_* . Between R_s and R_* , the radiation temperature decreases as $n^{\hat{\gamma}-1}$ where $\hat{\gamma} = 4/3$ is the adiabatic index of radiation, which gives $\bar{E} \propto r^{-2/3}$. The plasma has a small heat capacity (for $n \ll n_\gamma$) and tracks the radiation temperature. Electrons are thermally coupled to radiation via Compton scattering, and ions maintain thermal equilibrium with electrons via Coulomb collisions at a common low temperature $kT \lesssim 1$ keV.

The optical depth of the jet is given by

$$\tau_T = \frac{n \sigma_T r}{\Gamma} = \frac{L \sigma_T}{4\pi r m_p c^3 \Gamma^3} \approx r_{10}^{-1} L_{52} \Gamma_3^{-3}, \quad (4)$$

where $\sigma_T = 6.65 \times 10^{-25} \text{ cm}^2$ is Thomson cross section and $L = 4\pi r^2 \Gamma^2 n m_p c^3$ is the isotropic equivalent of the kinetic luminosity of the jet (it approximately equals the total luminosity at $r > R_s$). The photosphere radius $R_* \approx 10^{10} L_{52} \Gamma_3^{-3} \text{ cm}$ is larger than R_s for $\Gamma < 10^3 L_{52}^{1/4} r_{0,7}^{-1/4}$. The radiation luminosity released at the photosphere is $L_\gamma \approx (R_*/R_s)^{-2/3} L$, and the mean energy of the escaping photons is given by

$$\bar{E}(R_*) \sim \left(\frac{R_*}{R_s}\right)^{-2/3} \bar{E}_0 \approx 4 \Gamma_3^{8/3} L_{52}^{-5/12} r_{0,7}^{1/6} \text{ MeV}. \quad (5)$$

The thermal radiation creates a bright burst with MeV peak if $\Gamma \sim 10^3$. The burst is weak for slower flows: $L_\gamma \propto \Gamma^{8/3}$.

We have calculated the radiation spectrum emerging from the passively cooling jet using the Monte-Carlo code

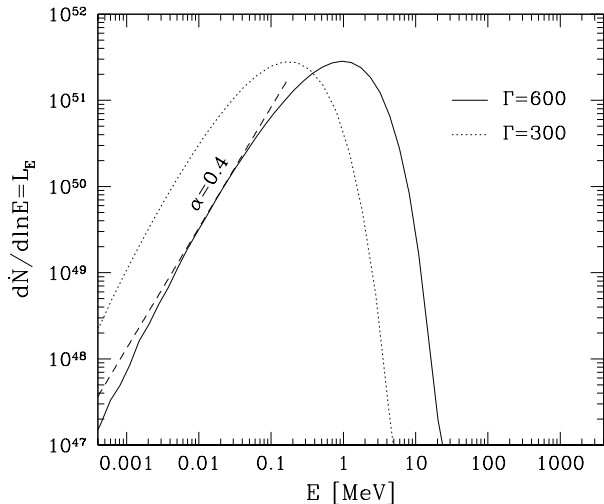


Figure 1. Photon spectrum emitted by a passively cooling jet to distant observers. The jet has kinetic luminosity $L = 10^{52}$ erg/s (isotropic equivalent) and effective initial size $r_0 = 10^7$ cm. The radiation spectrum has been calculated using the Monte-Carlo radiative transfer code. Two cases are shown: jets with asymptotic Lorentz factors $\Gamma = 600$ and 300 . *Dashed line* indicates the slope of the spectrum near 10 keV. The photon index $\alpha = 0.4$ corresponds to the slope of 1.4 in the figure. The spectrum cuts off exponentially at $E > E_{\text{peak}}$.

described in Appendix B. The scattering of the initial Planck spectrum was followed until the jet expanded to complete transparency. The spectrum of radiation received by distant observers is shown in Figure 1 for two example models. In qualitative agreement with the above estimates, the jet with $\Gamma = 600$ produces a bright GRB, whose spectrum peaks near MeV and cuts off exponentially. A couple of new details are shown by these simulations:

(i) Radiation emitted by passively cooling jets is not Planckian (contrary to the common assumption in GRB literature). Observer sees different parts of the photosphere at different angles, with different Doppler shifts. As a result, the low-energy slope of observed spectrum is softer than the Rayleigh-Jeans $\alpha = 1$ (photon index). Isotropic emission in the jet frame would produce $\alpha = 0$, and the exact α is controlled by the photon angular distribution near photosphere (e.g. $\alpha \approx 0.4$ near 10 keV in Fig. 1).

(ii) The standard description of adiabatic cooling predicts that radiation from a source at optical depth τ_T is cooled by the factor $A(\tau_T) = \tau_T^{-2/3}$ by the time the jet expands to its photospheric radius. The detailed transfer calculations give larger A . For example, $A(8) = 0.58$ instead of $8^{-2/3} = 1/4$ and $A(20) = 0.39$ instead of $20^{-2/3} \approx 0.14$. The scaling $A \propto \tau_T^{-2/3}$ is maintained at large $\tau_T > 10$.

The radiative transfer simulations illustrate and refine the standard fireball picture. They show that thermal radiation emitted by a passively cooling jet with $\Gamma > 500$ peaks at $E_{\text{peak}} \sim 1$ MeV and carries away a significant fraction ϵ of the jet energy (e.g. $\epsilon \approx 1/4$ for the model with $\Gamma = 600$ in Fig. 1). However, its spectrum cuts off exponentially at $E > E_{\text{peak}}$. Therefore, the model fails to explain the observed GRBs, whose spectra extend to energies $E \gg E_{\text{peak}}$. The extended high-energy emission requires an additional radiative mechanism.

3 NEUTRON COMPONENT AND COMPOUND FLOWS

The standard picture described in Section 2 is incomplete, because it misses the neutron component. In any plausible scenario of GRB trigger, matter in the central engine is dense, hot and neutron rich (Beloborodov 2003). In particular, neutrino-cooled accretion discs certainly have a high neutron fraction, as confirmed by recent detailed calculations (Chen & Beloborodov 2007). The neutron-rich matter is ejected in the jet and acquires a large Lorentz factor. The details of this process are uncertain (e.g. Metzger, Thompson & Quataert 2008). In all cases, neutrons and protons initially accelerate as a single fluid because they are coupled by frequent nuclear collisions.

Neutrons and protons tend to combine into helium when the ejecta temperature drops to 140 keV. This process, however, competes with rapid expansion and is marginally successful (Beloborodov 2003; see also Lemoine 2002 and Pruet, Woosley & Hoffman 2003 for similar calculations of the nuclear reaction network in GRB fireballs). Collimation of the jet generally helps nucleosynthesis because it slows down expansion (cf. Fig. 4 and 5 in Beloborodov 2003). However, even in cases where helium production is complete, some neutrons survive in the jet with a neutron excess, because helium production consumes equal numbers of n and p . Moreover, even if no neutrons survived the nucleosynthesis, free neutrons are later produced by internal shocks as a result of helium spallation in the shock-heated matter. Thus, there are good reasons to expect a neutron component in GRB jets.

Neutron-loaded jets generally tend to form *compound flows*: a slower neutron component with Lorentz factor Γ_n is embedded in a faster proton flow with Lorentz factor $\Gamma > \Gamma_n$. This occurs via two mechanisms:

(i) In jets that accelerate to $\Gamma \gtrsim 400$ neutrons do not develop the full Lorentz factor — their Γ_n saturates at a smaller value (Derishev et al. 1999; Fuller et al. 2000). For example, a baryonic flow accelerated to $\Gamma = 10^3$ will contain neutrons with $\Gamma_n \sim 10^2$. In spite of the significant difference in Lorentz factors, the two components move together without any separation for a long time, because their velocities relative to the central engine are almost equal (the velocities practically equal c). The ratio Γ/Γ_n starts to grow at the radius R_n where the collision timescale between neutrons and protons, $1/n\sigma c$, becomes longer than the expansion timescale, $r/c\Gamma$. Here both timescales are measured in the flow frame, n is the baryon number density, and $\sigma \sim 3 \times 10^{-26}$ cm² is the effective cross section of nuclear collisions. Γ_n remains constant at $r > R_n$, while the proton Lorentz factor Γ continues to grow until the saturation at radius R_s (Section 2). Formation of a compound flow is inevitable if $R_s \gtrsim R_n$, which translates to $\Gamma \gtrsim 400 L_{52}^{1/4} r_{0,7}^{-1/4}$.

(ii) In variable jets, internal shocks develop; however, the neutron component does not participate in the shocks. As a result, neutrons from the slow portions of the jet migrate across the shocks and penetrate the faster portions (Mészáros & Rees 2000). This internal mixing is caused by the short-timescale variability of the central engine that creates a non-uniform flow. The mixing occurs on scales $\delta r \sim r/\Gamma^2$, much smaller than the total thickness of the

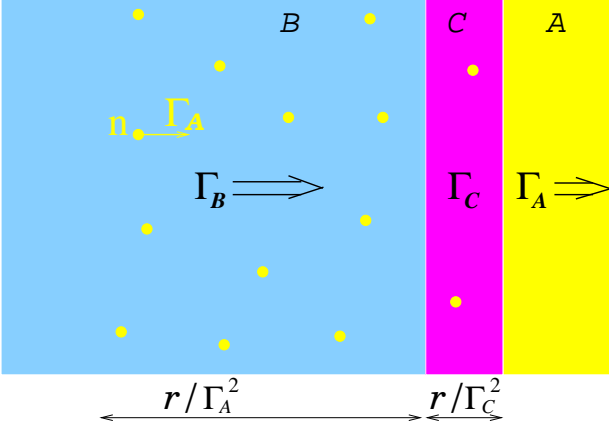


Figure 2. Faster flow \mathcal{B} sweeps slower flow \mathcal{A} and compresses it into a shocked shell \mathcal{C} . Neutrons from flow \mathcal{A} are not swept and instead penetrate flow \mathcal{B} . As a result a compound flow is formed: flow \mathcal{B} contains a slower neutron component with $\Gamma_n = \Gamma_A$. The penetration depth of neutrons is $\sim r/\Gamma_A^2$ in the lab frame; it is $(\Gamma_C/\Gamma_A)^2$ larger than the thickness of shocked region \mathcal{C} .

ejected flow. Large variations of Lorentz factors² produce a non-uniform compound flow with $\Gamma/\Gamma_n \gg 1$.

Neutron migration can be illustrated by the following simple model. Suppose neutron-loaded flow \mathcal{A} with Lorentz factor Γ_A is followed by faster flow \mathcal{B} with Lorentz factor $\Gamma_B \gg \Gamma_A$ (Fig. 2). A shocked region \mathcal{C} forms between the two flows; the shocked plasma has Lorentz factor Γ_C such that $\Gamma_A < \Gamma_C < \Gamma_B$. Initially, the neutron component of flow \mathcal{A} is coupled to protons by frequent collisions, so they behave essentially as a single fluid. When neutrons in flow \mathcal{A} become collisionally decoupled, they are not screened by region \mathcal{C} anymore and swiftly penetrate region \mathcal{B} with the relative Lorentz factor $\Gamma_{\text{rel}} = \frac{1}{2}(\Gamma_B/\Gamma_A + \Gamma_A/\Gamma_B) \approx \Gamma_B/2\Gamma_A$. The penetration/mixing length is $\sim (\Gamma_C/\Gamma_A)^2$ larger than the thickness of the shocked region \mathcal{C} .

Some of the penetrating neutrons collide with their new host flow. The collisions dissipate the relative kinetic energy $(\Gamma_{\text{rel}} - 1)m_p c^2$. The number of collisions per baryon of flow \mathcal{B} during the expansion timescale equals the ‘optical depth’ of the slow neutrons $\tau_n = n_n \sigma r / \Gamma_n$. At the beginning of neutron penetration $\tau_n \sim 1$ and a large heat is generated by collisions. The collisions decelerate flow \mathcal{B} from Γ_B to a new Γ , which is found from energy conservation in the static lab frame, $\tau_n \Gamma^2 / 2\Gamma_A \approx \Gamma_B$.³ This gives Γ that is lower than the original Γ_B by the factor $(\tau_n \Gamma_B / 2\Gamma_A)^{-1/2}$ as long as $\tau_n > \Gamma_{\text{rel}}^{-1}$.

In summary, GRB jets must contain a significant neutron component (unless they are essentially baryon-free and completely dominated by Poynting flux). When collisions between neutron and protons become rare, compound flows

with $\Gamma > \Gamma_n$ inevitably develop. Rare nuclear collisions in compound jets dissipate a huge energy, comparable to the total energy of the flow. The dissipation efficiency of nuclear collisions is $(\Gamma_{\text{rel}} - 1)\tau_n$, which can exceed 100 per cent as the collisionally decelerated jet tends to regain its initial Lorentz factor via adiabatic cooling and re-dissipate its energy. Below we explore how this dissipation affects the jet radiation.

4 RADIATIVE MECHANISM

Hereafter in this paper, we consider a simple model for compound jets: a neutron component with a single bulk Lorentz factor Γ_n is embedded in a fast proton component with constant Lorentz factor $\Gamma \gg \Gamma_n$. The proper densities of the neutron and proton components will be denoted by n_n and n , respectively.

4.1 Inelastic nuclear collisions

We consider collisions at radii where $\tau_n = n_n \sigma r / \Gamma_n < 1$,

$$r > R_n \equiv \frac{L_n \sigma}{4\pi m_p c^3 \Gamma_n^3} \approx 5 \times 10^{11} \left(\frac{L_n}{10^{52} \text{ erg/s}} \right) \left(\frac{\Gamma_n}{100} \right)^{-3} \text{ cm}, \quad (6)$$

where $L_n = 4\pi r^2 \Gamma_n^2 n_n m_p c^2$. Collisions between neutrons and protons are rare at $r > R_n$. The rate of collisions per unit volume (a Lorentz-invariant quantity) is given by

$$\dot{n} = n n_n \Gamma_{\text{rel}} \sigma c, \quad (7)$$

where $\Gamma_{\text{rel}} = \frac{1}{2}(\Gamma/\Gamma_n + \Gamma_n/\Gamma) \approx \Gamma/2\Gamma_n$. Collisions occur with $\Gamma_{\text{rel}} \gg 1$ and have a large inelastic fraction $f_{\text{inel}} \gtrsim 1/2$ (Amsler et al. 2008). The energy $f_{\text{inel}} \Gamma_{\text{rel}} m_p c^2$ is initially given to created mildly relativistic π^\pm and π^0 . The data on π^\pm multiplicity in p - p collisions are found in e.g. Breakstone et al. (1984) and refs. therein; similar multiplicity is expected for n - p collisions. The π^\pm , π^0 multiplicity is larger by the factor of 3/2; it slowly varies with Γ_{rel} and is typically 5-6.

The pions immediately decay: $\pi^\pm \rightarrow \mu^\pm + \nu_\mu \rightarrow e^\pm + \nu_e$ and $\pi^0 \rightarrow \gamma + \gamma$. The produced neutrinos escape with observed energies $\sim 0.1\Gamma$ GeV and carry away a fraction $f_\nu \sim 1/2$ of the pion energy.⁴ The remaining fraction is given to relativistic e^\pm and high-energy γ -rays, which quickly convert to e^\pm via γ - γ reaction. The net result of the inelastic collision is the injection of several e^\pm with a Lorentz factor $\gamma_0 \sim m_\pi/m_e \approx 300$ in the frame of the ambient plasma flow. The injected e^\pm carry a significant fraction $f_\pm = f_{\text{inel}}(1 - f_\nu) \approx 1/4$ of the collision energy $\Gamma_{\text{rel}} m_p c^2$.

The e^\pm are injected with a negative radial momentum in the frame of the proton flow. However, they lose this momentum and become quasi-isotropic in the plasma frame after one Larmor rotation. The magnetic field advected by the jet from the center of the explosion is almost exactly transverse to the jet direction (this is a consequence of magnetic flux conservation). Any reasonable magnetic field implies a very

² Large variations are usually assumed in the internal shock model to achieve a high dissipation efficiency (e.g. Beloborodov 2000). The picture of a variable jet is supported by observed strong variability in GRBs.

³ The decelerated flow with $\Gamma < \Gamma_B$ stores the heat of $\sim (\Gamma/2\Gamma_A)m_p c^2$ per baryon, and later tends to regain its initial Lorentz factor Γ_B as the heat converts back to bulk kinetic energy via adiabatic cooling on the expansion timescale.

⁴ On average, neutrinos take $\sim 3/4$ of π^\pm energy. The average fraction of π^\pm and π^0 energy that is wasted to neutrinos may be estimated as $f_\nu \sim (2/3)(3/4) = 1/2$.

short gyration timescale $eB/m_e c \gamma_0$, and the net momentum of injected e^\pm is immediately communicated to the plasma and vanishes in the plasma frame.

The energy of e^\pm injected per unit volume per unit time is approximately equal to $f_\pm \Gamma_{\text{rel}} m_p c^2 \dot{n}$. Practically all of this energy is quickly converted to radiation (see Section 4.2 below). As a result, the plasma accumulates radiation energy density with rate

$$\dot{Q}_{\text{nth}} = f_\pm \Gamma_{\text{rel}} m_p c^2 \dot{n}. \quad (8)$$

Here dot denotes derivative with respect to time in the plasma rest frame, d/dt' . Subscript 'nth' stands for radiation produced by nonthermal e^\pm that are generated by nuclear collisions. Using equation (7) and $d/dt' = c\Gamma d/dr$ one finds

$$\frac{1}{nm_p c^2} \frac{dQ_{\text{nth}}}{d \ln r} = \frac{f_\pm}{4} \frac{\Gamma}{\Gamma_n} \tau_n \approx \frac{1}{16} \frac{\Gamma}{\Gamma_n} \frac{R_n}{r}. \quad (9)$$

4.2 Radiative cooling of injected e^\pm

The e^\pm injected by nuclear collisions have a large Lorentz factor $\gamma_0 \sim m_\pi/m_e$ and immediately radiate their energy via Compton and/or synchrotron cooling.

4.2.1 Compton cooling

The timescale for Compton cooling of an electron with Lorentz factor γ by radiation with energy density U_γ is⁵

$$t_C = \frac{3m_e c}{4U_\gamma \sigma_T \gamma}. \quad (10)$$

Radiation is initially present in GRB jets (Section 2), and U_γ is further increased as the radiation absorbs the energy of injected e^\pm . Compton cooling timescale is shorter than the timescale of jet expansion $t_{\text{exp}} = r/c\Gamma$. Their ratio is

$$\frac{t_C}{t_{\text{exp}}} = \frac{3}{4l\gamma}, \quad (11)$$

where

$$l \equiv \frac{U_\gamma}{m_e c^2} \sigma_T \frac{r}{\Gamma} \quad (12)$$

is the dimensionless 'compactness' parameter of the radiation field. One can express l as

$$l = \frac{m_p}{m_e} \epsilon \tau_p, \quad \epsilon \equiv \frac{U_\gamma}{nm_p c^2}. \quad (13)$$

Here ϵ is the fraction of the jet energy that is carried by radiation ($\epsilon > 0.1$ for the model proposed in this paper), and

$$\tau_p \equiv \frac{\sigma_T n r}{\Gamma} = \frac{\sigma_T}{\sigma} \frac{n}{n_n} \frac{\Gamma_n}{\Gamma} \tau_n \approx \left(\frac{L}{5L_n} \right) \left(\frac{\Gamma}{5\Gamma_n} \right)^{-3} \tau_n. \quad (14)$$

The compactness l is large in the heating region $\tau_n \lesssim 1$, and hence Compton cooling is fast, $t_C \ll t_{\text{exp}}$.

⁵ This estimate assumes Thomson scattering, i.e. neglects the Klein-Nishina correction to the scattering cross section. The peak of GRB radiation is $E'_{\text{peak}} \sim \text{MeV}/\Gamma \sim \text{keV}$ in the jet frame. Since $E'_{\text{peak}} \gamma < m_e c^2$ for all $\gamma \leq \gamma_0$, most of the scattering by e^\pm occurs in Thomson regime. Exact calculations of radiative transfer with the full Klein-Nishina cross section are performed in Section 5.

The large compactness has another implication. Photons that are scattered by relativistic e^\pm to energies $E' \gg 1$ MeV in the jet frame will not survive and convert to secondary e^\pm via reaction $\gamma + \gamma \rightarrow e^+ + e^-$. The development of e^\pm cascade that accompanies Compton cooling of relativistic particles (Appendix A) is described in detail by Svensson (1987) and Lightman & Zdziarski (1987). In this paper, the cascade is modeled numerically with the Monte-Carlo code. The typical multiplicity of secondary e^\pm \mathcal{M}_s is comparable to 50. The total multiplicity of e^\pm created following one nuclear collision is

$$\mathcal{M} = \mathcal{M}_0 \mathcal{M}_s \sim 10^2, \quad (15)$$

where

$$\mathcal{M}_0 = \frac{f_\pm \Gamma_{\text{rel}} m_p}{\gamma_0 m_e} \sim \frac{3}{4} \frac{\Gamma}{\Gamma_n} \quad (16)$$

is the multiplicity of 'primary' e^\pm injected with Lorentz factor $\gamma_0 \sim m_\pi/m_e$ following a nuclear collision.

4.2.2 Synchrotron cooling

In the presence of magnetic fields, the injected e^\pm also experience synchrotron losses. The synchrotron cooling timescale is similar to equation (10) except that U_γ in this equation is replaced by magnetic energy density U_B . The synchrotron losses dominate if $U_B > U_\gamma$. The magnetic energy density in the jet frame may be written as

$$U_B = \frac{B^2}{8\pi} = \frac{\epsilon_B L}{4\pi r^2 \Gamma^2 c}, \quad (17)$$

where ϵ_B is the magnetic fraction of the jet energy. The typical energy of synchrotron photons in the plasma frame is $E'_s = 0.3 \gamma_0^2 \hbar e B / m_e c$. The corresponding energy in the lab frame, $E_s \approx \Gamma E'_s$, is given by

$$E_s \approx 0.3 \gamma_0^2 \frac{\hbar e}{m_e c r} \left(\frac{2\epsilon_B L}{c} \right)^{1/2} \approx 200 r_{12}^{-1} \epsilon_B^{1/2} L_{52}^{1/2} \text{ keV}, \quad (18)$$

where we substituted $\gamma_0 \approx m_\pi/m_e \approx 300$. We are interested in radii $r \gtrsim R_n$ where the collisional dissipation peaks (eq. 6). Jets for which synchrotron cooling is relevant (i.e. where it can compete with Compton cooling) have large ϵ_B ; then the synchrotron photons have energy comparable to MeV. Interestingly, the characteristic energy E_s is near the peak of observed GRB spectra. This offers an additional mechanism for the preferential peak position at 0.1-1 MeV.

Synchrotron emission from particles with low $\gamma \lesssim 5$ is self-absorbed. These particles cannot be cooled by the synchrotron mechanism; they are Compton cooled.

4.3 Optical depth of the jet

In view of the strong e^\pm loading and the large cross section for photon scattering $\sigma_T \gg \sigma$, one might expect a huge optical depth τ_T where the collisional heating takes place. Note, however, that $\tau_T \propto \Gamma^{-3}$ while $\tau_n \propto \Gamma_n^{-3}$. In compound flows $(\Gamma/\Gamma_n)^{-3} \ll 1$; as a result, the collisionally heated jet with $\tau_n \lesssim 1$ has a moderate τ_T .

If no e^\pm pairs were created, the optical depth of the compound flow would equal τ_p (eq. 14), which may be smaller than unity at $r \gtrsim R_n$. The actual optical depth is enhanced and dominated by e^\pm created by the nonthermal cascade

(Derishev et al. 1999). The continually injected e^\pm quickly cool down and accumulate at relatively low energies, forming a thermalized population that maintains Maxwellian distribution via frequent Coulomb collisions between e^\pm . The rate of e^\pm supply can be conveniently written as

$$\dot{n}_\pm = \mathcal{M}\dot{n} = \frac{Y \dot{Q}_{\text{nth}}}{m_e c^2}, \quad (19)$$

where $\dot{Q}_{\text{nth}} = f_\pm \Gamma_{\text{rel}} m_p c^2 \dot{n}$ is the rate of energy injection in primary e^\pm , and $Y = \mathcal{M}_s/\gamma_0$ is the ‘pair yield’ of the cascade. A minimum $Y_{\text{min}} \sim \gamma_0^{-1}$ would be obtained when counting only the primary e^\pm from pion decay. This may be appropriate for strongly magnetized jets where the synchrotron cooling of e^\pm strongly dominates over Compton cooling ($U_B \gg U_\gamma$). In moderately or weakly magnetized jets with $U_B \lesssim U_\gamma$, the development of e^\pm cascade gives $Y = \mathcal{M}_s/\gamma_0 \sim 0.1$.

Let n_\pm be the density of accumulated thermalized pairs. Their annihilation rate is given by

$$\dot{n}_{\text{ann}} = \frac{3}{16} \sigma_T c n_\pm^2. \quad (20)$$

This expression assumes $n_\pm > n$ and $kT < m_e c^2$; both assumptions are valid where annihilation is significant. The density of accumulated e^\pm evolves according to equation

$$\frac{\Gamma c}{r^2} \frac{d}{dr} (r^2 n_\pm) = \dot{n}_\pm - \dot{n}_{\text{ann}}. \quad (21)$$

At the beginning of collisional heating, \dot{n}_\pm and \dot{n}_{ann} are both larger than the left side of equation (21), and the equilibrium $\dot{n}_\pm \approx \dot{n}_{\text{ann}}$ is established,

$$Y f_\pm \Gamma_{\text{rel}}^2 \frac{m_p}{m_e} \sigma c n_n n = \frac{3}{16} \sigma_T c n_\pm^2, \quad (22)$$

which gives

$$\tau_T(r) \equiv \frac{n_\pm \sigma_T r}{\Gamma} = \left(\frac{4}{3} \frac{m_p}{m_e} \frac{\sigma_T}{\sigma} f_\pm Y \frac{L}{L_n} \right)^{1/2} \frac{\Gamma_n}{\Gamma} \tau_n, \quad (23)$$

or, using $\tau_n = R_n/r$ and $f_\pm \approx 1/4$,

$$\tau_T(r) = \tau_0 \frac{R_n}{r}, \quad \tau_0 \approx 20 \left(Y \frac{L}{L_n} \right)^{1/2} \left(\frac{\Gamma}{5\Gamma_n} \right)^{-1}. \quad (24)$$

τ_T stays near the equilibrium value $\propto \tau_n$ even after the annihilation timescale becomes long and the e^\pm population freezes-out. This is the result of a coincidence: the annihilation equilibrium gives $\tau_T \propto r^{-1}$, which is also maintained when $\dot{n}_\pm = \dot{n}_{\text{ann}} = 0$. Therefore, equation (24) remains valid even at late stages when the jet becomes transparent to radiation.

The e^\pm optical depth is maximum at the beginning (and peak) of collisional dissipation when $\tau_n \sim 1$. At this stage, Γ/Γ_n is limited by the deceleration effect of collisions (see the end of Section 3). In particular, the collision of flows \mathcal{A} and \mathcal{B} considered in Section 3 gives a compound flow with $\Gamma_n = \Gamma_{\mathcal{A}}$ and $\Gamma/\Gamma_n \approx (2\Gamma_{\mathcal{B}}/\Gamma_{\mathcal{A}})^{1/2}$. Substituting $L = L_{\mathcal{B}}$, $L_n \sim L_{\mathcal{A}}$, we find

$$\tau_0 \approx 20 \left(\frac{Y}{0.1} \right)^{1/2} \left(\frac{\Gamma_{\mathcal{A}}}{\Gamma_{\mathcal{B}}} \frac{L_{\mathcal{B}}}{L_{\mathcal{A}}} \right)^{1/2}. \quad (25)$$

It is reasonable to suppose $L_{\mathcal{B}}/L_{\mathcal{A}} > 1$ when $\Gamma_{\mathcal{B}}/\Gamma_{\mathcal{A}} > 1$ and expect $(\Gamma_{\mathcal{B}} L_{\mathcal{A}}/\Gamma_{\mathcal{B}} L_{\mathcal{B}})^{1/2} \sim 1$ within a factor of a few. Then equation (25) predicts the nearly unique $\tau_T(R_n) = \tau_0 \sim 20$ for different GRB jets. The moderate optical depth

at $r \gtrsim R_n$ implies that the produced radiation is not buried in the opaque jet. As demonstrated by the radiative transfer simulations in Section 5, it creates a powerful burst escaping to distant observers.

4.4 Heating of thermalized e^\pm by ions

The thermalized e^\pm population in the jet tends to the thermal equilibrium with radiation. If no mechanism heats e^\pm , they would quickly reach the equilibrium at temperature $T_e = T_C$, where $kT_C \sim \text{keV}$. This, however, does not happen because e^\pm are continually heated by Coulomb collisions with protons. As a result, the e^\pm temperature T_e is maintained above T_C . Its value is estimated below.

Nuclear collisions with $\Gamma_{\text{rel}} > 1$ inevitably heat the proton component of the jet to a relativistic temperature⁶ $kT_p \sim m_p c^2$. The temperature of the accumulated e^\pm population is kept at a much smaller value by Compton cooling. In this two-temperature plasma, Coulomb collisions tend to transfer energy from ions to e^\pm . The rate of energy transfer (measured in the plasma frame) is given by (Spitzer 1956),

$$\dot{Q}_{ep} = \frac{U_p}{t_{ep}}, \quad t_{ep} = \sqrt{\frac{\pi}{2}} \frac{m_p}{m_e} \frac{(\Theta_e + \Theta_p)^{3/2}}{\sigma_T c \ln \Lambda n_\pm}, \quad (26)$$

where $\Theta_e \equiv kT_e/m_e c^2$, $\Theta_p = kT_p/m_p c^2$, $\ln \Lambda \approx 15$ is the Coulomb logarithm, $U_p = nkT_p/(\hat{\gamma} - 1)$ is the proton energy density, and $\hat{\gamma}$ is the adiabatic index of the proton gas; $\hat{\gamma} = 5/3$ for $\Theta_p \ll 1$ and $\hat{\gamma} = 4/3$ for $\Theta_p \gg 1$. In the collisionally heated jet, Θ_p is comparable to 1. Convenient approximate formulas relate $\hat{\gamma}$ and Θ_p to the dimensionless thermal energy per proton, $u \equiv U_p/nm_p c^2$,

$$\hat{\gamma} - 1 = \frac{1}{3} \left(1 + \frac{1}{1+u} \right), \quad \Theta_p = (\hat{\gamma} - 1)u. \quad (27)$$

These relations have better than 5 per cent accuracy.

The heat gained by electrons from protons during the timescale of jet expansion $t_{\text{exp}} = r/c\Gamma$ is $\dot{Q}_{ep} r/c\Gamma = dQ_{ep}/d \ln r$. One then finds,

$$\frac{1}{nm_p c^2} \frac{dQ_{ep}}{d \ln r} = \sqrt{\frac{2}{\pi}} \frac{m_e}{m_p} \ln \Lambda (\hat{\gamma} - 1)^{-1} \Theta_p^{-1/2} \tau_T. \quad (28)$$

We neglected here Θ_e compared with $\Theta_p \sim 1$ (this is a valid approximation, see eq. 32 below). For relevant $u = 0.5 - 2$, $dQ_{ep}/d \ln r$ weakly depends on u and is approximately given by

$$\frac{1}{nm_p c^2} \frac{dQ_{ep}}{d \ln r} \approx 0.02 \tau_T. \quad (29)$$

It is useful to compare \dot{Q}_{ep} with \dot{Q}_{nth} (Section 4.1). From equations (9), (29), and (24) one finds,

$$\frac{\dot{Q}_{ep}}{\dot{Q}_{\text{nth}}} \approx \left(\frac{L}{5L_n} \right)^{1/2} \left(\frac{\Gamma}{5\Gamma_n} \right)^{-2} \left(\frac{Y}{0.1} \right)^{1/2}. \quad (30)$$

The thermal and nonthermal heating rates are comparable.

The e^\pm do not keep the heat Q_{ep} received from protons. Instead, they immediately pass it to radiation via Compton scattering and remain at a temperature $kT_e \ll Q_{ep}/n_\pm$.

⁶ Nuclear collisions also create a hot neutron component moving with the bulk Lorentz factor Γ . The density of hot neutrons is smaller than the density of protons by the factor τ_n .

The value of T_e is found from the balance between Coulomb heating and Compton cooling of e^\pm ,

$$\frac{3}{2} n_\pm \frac{k(T_e - T_C)}{t_C} = \dot{Q}_{ep}, \quad (31)$$

where t_C is given by equation (10) with $\gamma \approx 1$. We have neglected the adiabatic cooling of e^\pm because its rate is smaller than Coulomb heating and Compton cooling rates by the factor $t_C/t_{\text{exp}} \ll 1$. Then we find

$$\Theta_e \approx \frac{\ln \Lambda}{\sqrt{2\pi}} \frac{m_e/m_p}{(\hat{\gamma} - 1)\Theta_p^{1/2}} \approx \frac{0.01}{\epsilon}. \quad (32)$$

Temperature T_e is well above T_C (and therefore T_C is neglected compared with T_e in eq. 32).

Kompaneets' y -parameter of thermal e^\pm is given by

$$y = 4\tau_T \Theta_e = \frac{2}{U_\gamma} \frac{dQ_{ep}}{d \ln r}. \quad (33)$$

It is close to unity, which implies that Compton cooling of e^\pm occurs in the unsaturated regime. Thermal Comptonization has an important effect on the radiation spectrum, which is computed in Section 5.

4.5 Radiative efficiency of photospheric emission

The evolution of radiation density U_γ (measured in the plasma comoving frame) is given by equation

$$\frac{1}{r^2} \frac{d}{d \ln r} (r^2 U_\gamma) = \left(\frac{dU_\gamma}{d \ln r} \right)_{\text{ad}} + \frac{dQ_{ep}}{d \ln r} + \frac{dQ_{\text{nth}}}{d \ln r}. \quad (34)$$

The first term on the right side of this equation describes the adiabatic cooling of radiation; it equals $-(2/3)U_\gamma$ in the opaque zone and 0 in the transparent zone (the exact behavior of this term near photosphere is obtained from the numerical simulation of radiative transfer). The second and third terms on the right side represent the energy received by e^\pm plasma and converted to radiation. Since practically all of the energy received by e^\pm is passed to radiation, these terms effectively serve as sources of radiation energy. Heating of the thermalized e^\pm population by Coulomb collisions with protons $dQ_{ep}/d \ln r$ is given by equation (29). Energy injection into the nonthermal e^\pm tail $dQ_{\text{nth}}/d \ln r$ is given by equation (9). Substituting these expressions we obtain the equation for $\epsilon \equiv U_\gamma/nm_p c^2$,

$$x \frac{d\epsilon}{dx} = -q(x) \epsilon + \frac{a_{\text{th}} + a_{\text{nth}}}{x}, \quad (35)$$

where $a_{\text{th}} = 0.02\tau_0$ and $a_{\text{nth}} = f_\pm \Gamma_{\text{rel}}/2$ are constants, $x \equiv r/R_n$, and $q(x) \equiv -(d \ln U_\gamma / d \ln r)_{\text{ad}}$ is a dimensionless function that equals $2/3$ in the optically thick zone $\tau_T \gg 1$ and approaches 0 at the photosphere. The quantity ϵ is the fraction of the jet energy carried by radiation; it can also be written in the lab frame as

$$\epsilon = \frac{L_\gamma}{L}, \quad (36)$$

where $L_\gamma = 4\pi r^2 \Gamma^2 U_\gamma c$ is the isotropic equivalent of radiation luminosity, and $L = 4\pi r^2 \Gamma^2 n m_p c^3$ is the isotropic equivalent of the jet kinetic luminosity.

In the optically thick zone, where $q \approx 2/3$, equation (35) can be solved analytically for $\epsilon(x)$,

$$\epsilon(x) = \frac{\epsilon_1 + 3a}{x^{2/3}} - \frac{3a}{x}, \quad 1 < x < \frac{R_\star}{R_n}, \quad (37)$$

where $\epsilon_1 \equiv \epsilon|_{r=R_n}$ and $a = a_{\text{th}} + a_{\text{nth}}$. The solution may be used to estimate ϵ at the photosphere, $x_\star = R_\star/R_n = \tau_0$. For jets with small ϵ_1 one obtains

$$\epsilon_\star \approx \left(0.06 \tau_0^{1/3} + \frac{0.2}{\tau_0^{2/3}} \frac{\Gamma}{\Gamma_n} \right) \left(1 - \frac{1}{\tau_0^{1/3}} \right) \approx 0.1 + 0.02 \frac{\Gamma}{\Gamma_n}, \quad (38)$$

where we substituted $\tau_0 \approx 20$ (Sect. 4.3). Equation (38) estimates the net radiative efficiency of collisional heating in jets with $\Gamma \gg \Gamma_n$, taking into account the adiabatic cooling of radiation until the jet expands to transparency.⁷ The two terms represent the contributions from the Coulomb heating of thermalized e^\pm and the nonthermal e^\pm injection. For typical $\Gamma/\Gamma_n \sim 3-10$ equation (38) gives the total radiative efficiency $\epsilon_\star = 0.2-0.3$, with the thermal part comparable to the nonthermal part (cf. also eq. 30).

5 RADIATION SPECTRA FROM COLLISIONALLY HEATED JETS

We assume that the jet cools passively at $r < R_n$ and its thermal radiation evolves as described in Section 2. The collisional heating begins at radius R_n (eq. 6) and quickly loads the jet with energetic e^\pm . Scattering of radiation by the injected e^\pm dramatically changes the photon spectrum, which will be released at the photosphere.

Consider a weakly magnetized jet with $U_B \ll U_\gamma$, when the synchrotron cooling of e^\pm is negligible. Then the GRB spectrum forms via Comptonization of already existing thermal photons advected from the center of the explosion. Scattering conserves photon number and the average photon energy \bar{E} in the lab frame can be expressed as (cf. eqs. 2 and 3)

$$\bar{E} = \frac{\epsilon \Gamma n m_p c^2}{n_\gamma} = \epsilon \bar{E}_0 \approx 4 \epsilon r_{0.7}^{-1/2} L_{52}^{1/4} \text{ MeV}, \quad (39)$$

where $\epsilon = L_\gamma/L$ is the fraction of jet energy carried by radiation. The relation (39) is common for all Comptonization models of GRBs (e.g. Rees & Mészáros 2005). It naturally explains the observed $\bar{E} \sim \text{MeV}$, assuming a reasonable radiative efficiency $\epsilon \gtrsim 0.1$. In the collisionally heated jet, \bar{E} grows as photons receive energy via two branches of heating: thermal and nonthermal (Section 4). The corresponding heating rates *per photon* give

$$\left(\frac{d\bar{E}}{d \ln r} \right)_{\text{th}} \approx 0.02 \tau_0 \bar{E}_0 \frac{R_n}{r}, \quad (40)$$

$$\left(\frac{d\bar{E}}{d \ln r} \right)_{\text{nth}} \approx \frac{1}{16} \frac{\Gamma}{\Gamma_n} \bar{E}_0 \frac{R_n}{r}, \quad (41)$$

where \bar{E}_0 is given by equation (3). The heating rates and the adiabatic cooling determine the evolution $\bar{E}(r)$ in the collisionally heated jet.⁸ However, the known \bar{E} does not determine the shape of the radiation spectrum. The spectrum depends on the details of Comptonization that need to be calculated.

⁷ Equation (38) assumes the adiabatic cooling $\propto r^{-2/3}$ at all $r < R_\star$. It overestimates the cooling effect – the exact radiative transfer gives less cooling (see Section 2). Therefore, equation (38) underestimates ϵ_\star by a factor ~ 2 .

⁸ Since $\bar{E}/\bar{E}_0 = \epsilon$ for a jet with a conserved photon number, the equation for $\bar{E}(r)$ is immediately obtained from eq. (35).

The radiation spectra produced by Compton cooled e^\pm cascades were previously studied in detail in the context of AGN accretion discs (e.g. Svensson 1987; Lightman & Zdziarski 1987; see also Appendix A). The model was developed for static sources. Comptonization of radiation in relativistic jets is different for two reasons. First, the optical depth evolves as the jet expands. Second, the GRB radiation moves together with the plasma and remains embedded in it until the jet reaches $r \sim R_\Delta \sim \Gamma^2 \Delta \sim 10^{16}$ cm (here $\Delta/c \sim 1 - 10$ s is the typical duration of GRB jets). The collisional heating operates at much smaller radii $r \sim (1 - 10^2) R_n \ll R_\Delta$, and the entire history of heating and Comptonization is ‘recorded’ in the radiation field before it escapes the jet. The spectrum received by distant observers is the net result of multi-radius (multi-optical-depth) Comptonization in the expanding jet. In this respect, GRBs are similar to the relict radiation in the expanding universe.

The cooling rate of e^\pm and their energy distribution at any given location depend on the local radiation field. Therefore, the evolution of radiation and e^\pm plasma must be calculated self-consistently. This is achieved using the numerical code described in Appendix B. The code is based on the Monte-Carlo method that solves for the radiative transfer in a jet with given e^\pm distribution. The consistency of the radiation field with the e^\pm distribution at all radii is achieved via iterations. As a result, the code finds, for a given history of heating, the spectrum of photons received by distant observers.

As a typical example, consider the jet from Section 2 with $\Gamma = 600$, $L = 10^{52}$ erg/s, and $r_0 = 10^7$ cm, but now let it contain a neutron component with $\Gamma_n = 100$ and $L_n = 10^{51}$ erg/s. The collisional heating begins at radius $R_n \sim 10^{11}$ cm (eq. 6). Just before the onset of heating and e^\pm creation, the passively cooling jet has $\bar{E}(R_n) \approx 1$ MeV. The optical depth of the jet after the onset of collisional heating is $\tau_r(r) = (R_n/r)\tau_0$ with $\tau_0 \approx 20$ (eq. 24). The heating rates in equations (40) and (41) are almost exactly equal for our example model: $(d\bar{E}/d\ln r)_{\text{nth}} \approx (d\bar{E}/d\ln r)_{\text{th}} \approx 1.5(R_n/r)$ MeV. Figure 3 shows the spectrum of emitted radiation for this illustrative model. Although it is not obvious from the figure, the spectrum has two components:

(i) Most photons are multiply scattered by the optically thick thermalized e^\pm population and never scattered by the optically thin nonthermal tail. This thermal Comptonization creates high-energy emission with the spectrum slope $\beta \sim 2 - 3$. The slope is determined by Kompaneets’ y -parameter, which is regulated to $y \sim 1$ in the heated jets (Section 4.4). Thermal Comptonization dominates the emitted spectrum at energies up to 0.1 GeV.

(ii) A small fraction of photons are additionally scattered by the nonthermal tail of e^\pm distribution, which strongly boosts their energy. The nonthermal component dominates the radiation spectrum at $\gtrsim 0.1$ GeV. It cuts off above GeV (above a few MeV in the plasma frame) because of $\gamma\gamma$ absorption.

A special feature of collisional heating is that the energy of the two spectral components (thermal and nonthermal) are comparable. The 0.1-1 GeV nonthermal bump does not necessarily stand out as a separate component. It typically appears as a modest hump that smoothly extends the spectrum through 100 MeV to the GeV range. This hump

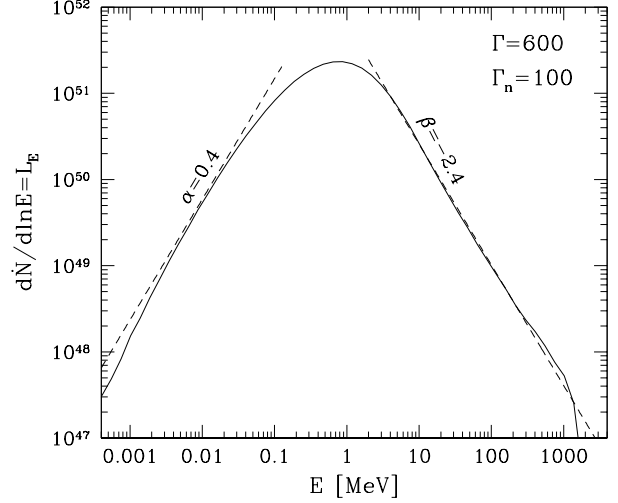


Figure 3. Photon spectrum emitted by the collisionally heated jet. The jet has $L = 10^{52}$ erg/s, $r_0 = 10^7$ cm, $\Gamma = 600$ (same as in Fig. 1), and carries neutrons with $\Gamma_n = 100$. Dashed lines indicate the slopes of the spectrum near 10 keV (photon index $\alpha \approx 0.4$) and above a few MeV (photon index $\beta \approx -2.4$). The correction due to the cosmological redshift of the burst z is not included. The redshifted spectrum will peak at $(1+z)^{-1}$ MeV instead of 1 MeV. A similar phenomenological spectrum is usually proposed to fit GRB observations (Band et al. 2009).

is broad and smooth because it is partly downscattered in the optically thick plasma before the jet expands to transparency and releases the radiation.

Most of collisional heating occurs when the jet is still opaque to radiation. The Comptonized radiation is released at the photosphere R_* and can be called ‘photospheric emission.’ The average energy of escaping photons in the model shown in Figure 3 is $\bar{E} \approx 2$ MeV, which is half of $\bar{E}_0 \approx 4$ MeV. This means that the net radiation efficiency of the burst is $\sim 50\%$, i.e. the photospheric emission carries about half of the jet energy.⁹

The ratio of the thermal and nonthermal components w is controlled by Γ/Γ_n and τ_0 : $w \approx 0.3\tau_0\Gamma_n/\Gamma$ (cf. eqs. 40 and 41), where τ_0 is likely to stay near 20 within a factor of a few (Section 4.3). The parameter w controls the shape of the emitted spectrum at high energies.

To investigate the sensitivity of the model predictions to expected variations in w , let us consider two models with equal $\tau_0 = 20$ and different $\Gamma/\Gamma_n = 12$ and $\Gamma/\Gamma_n = 3$. The model with $\Gamma/\Gamma_n = 12$ has $w = 2$, $(d\bar{E}/d\ln r)_{\text{th}} = 1(R_n/r)$ MeV and $(d\bar{E}/d\ln r)_{\text{nth}} = 2(R_n/r)$ MeV. The model with $\Gamma/\Gamma_n = 3$ has $w = 1/2$, $(d\bar{E}/d\ln r)_{\text{th}} = 2(R_n/r)$ MeV and $(d\bar{E}/d\ln r)_{\text{nth}} = 1(R_n/r)$ MeV. The results are shown in Figure 4. They are similar: in both models the high-energy spectrum is close to a power law. Its photon index is $\beta = -2.3$ for the model with $w = 2$ (which is close to the spectrum in Fig. 3 where $w = 1$ and $\beta = -2.4$). The model with $w = 1/2$ has a steeper spectrum

⁹ The energy given to photons by the collisional heating in the region $R_n < r < R_*$ is 2×1.5 MeV in this model. Together with the initial 1 MeV per photon at R_n this would make $\bar{E} = 4$ MeV, if there were no adiabatic cooling. The adiabatic cooling at $r < R_*$ reduces \bar{E} by a factor of 2.

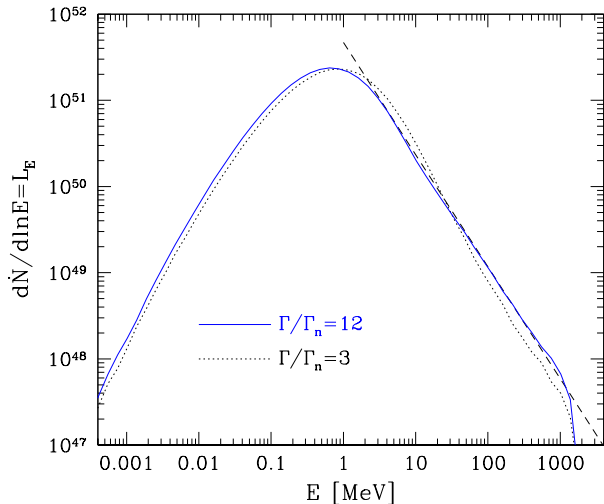


Figure 4. Photon spectrum emitted by two collisionally heated jets similar to the model in Fig. 3, but with different $\Gamma/\Gamma_n = 12$ (blue solid curve) and $\Gamma/\Gamma_n = 3$ (black dotted curve). Dashed line shows the slope that corresponds to photon index $\beta = -2.3$.

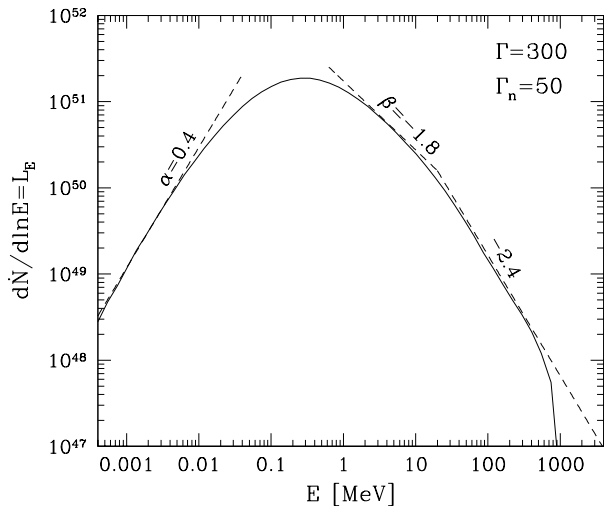


Figure 5. Photon spectrum emitted by the jet with the same L , r_0 , and Γ/Γ_n as in Fig. 3, but with a lower $\Gamma = 300$. Dashed lines show the slopes of different parts of the spectrum; the corresponding photon index is indicated next to the line.

$\beta \approx 2.5$. We conclude that, for the typical expected w , the spectrum between MeV and GeV is close to a power-law with $\beta \sim 2.3 - 2.5$. Large $w \gg 1$ would lead to stronger nonthermal bumps at $E \gtrsim 100$ MeV. Small $w \ll 1$ would give spectra dominated by thermal Comptonization, which steepen at $E \gtrsim 100$ MeV.

The results shown in Figures 3 and 4 hold for jets with large $\Gamma \gtrsim 500$. Jets with smaller Γ produce somewhat different Comptonized spectra. This is illustrated in Figure 5. In this model, the jet has $\Gamma = 300$, and all other parameters are the same as in Figure 3; in particular $\Gamma/\Gamma_n = 6$, which corresponds to $\Gamma_n = 50$. The main difference caused by the smaller Γ is that the radiation temperature prior to the onset of heating drops to a low value (the adiabatically cooled T scales as $\Gamma^{8/3}$, see Section 2). The collisional heat-

ing is still strong in the model, giving a similar high radiative efficiency and a high $\bar{E} \approx 1.5$ MeV. However, the shape of emitted spectrum changes. Its E_{peak} is smaller and the spectrum has the large \bar{E} due to a broad bump with a running slope between 0.4 MeV and 20 MeV.

This calculation illustrates a general property of Comptonization models for GRB emission. Photospheric models with efficient volume heating do not give the simple Band-type spectrum with the MeV break if the radiation temperature dropped much below MeV prior to the heating. The cooling stage creates the exponential break at a low energy $E \ll 1$ MeV (Sect. 2). Then heating and Comptonization increases \bar{E} back to \sim MeV; however, the recovery of \bar{E} is achieved only by hardening the spectrum above the break, without a significant shift in the break position. This is a general property of unsaturated Comptonization.¹⁰

Two additional effects can change the observed spectra, in particular the slope α at $E < E_{\text{peak}}$. (i) A modest magnetic field adds synchrotron emission, which peaks at $E_s \lesssim 1$ MeV (eq. 18) and can dominate at $E < E_{\text{peak}}$ because the synchrotron spectrum is relatively soft, $\alpha = -1/2$. (ii) Variable jets consist of many thin shells with different parameters, and their radiation spectra vary on timescales as short as ms (in observer time). The superposition of many different instantaneous spectra is observed when the true instantaneous spectrum is not time-resolved. This can reduce the observed α (e.g. Ryde & Svensson 1999).

6 DISCUSSION

6.1 Photospheric emission

Formation of GRB spectra is a long-standing problem. Most of the previous work focused on the optically thin internal-shock model (see Bosnjak, Daigne & Dubus 2009 for recent detailed calculations). The model posits that the observed γ -rays are produced by electrons accelerated in the shocks and introduces a few phenomenological parameters of this process. Recent plasma simulations significantly advanced the model, however some key issues remained unsettled: Should a high radiative efficiency be expected? Why do the reported spectra of GRBs usually peak near MeV and exhibit a broken power-law shape? Why are the low-energy slopes of some GRBs so hard ($\alpha \gtrsim 0$, much harder than e.g. synchrotron emission)? As a possible solution, it was hypothesized that GRB spectra include a bright photospheric component which results from strong sub-photospheric heating (e.g. Rees & Mészáros 2005 and refs. therein).

The results of the present paper support the photospheric origin of GRB radiation. The sub-photospheric collisional heating is robust in neutron-loaded jets. It controls the position of the photosphere R_* and peaks at radii $\sim 0.1R_*$. It is quite remarkable that the simple addition of a neutron component to the standard fireball picture completely changes the photospheric radiation and makes it consistent with observations (Figs. 3 and 4) without invoking unknown parameters apart from the Lorentz factor and the

¹⁰ Saturated Comptonization ($y \gg 1$) would shift the peak of the spectrum, however it appears to be not relevant to GRBs as it requires strong photon starvation.

initial radius of the jet r_0 . The radiative efficiency of collisional heating is large: it converts $\gtrsim 30$ per cent of the jet energy to photospheric radiation, regardless the strength of the magnetic field. If the jet is strongly magnetized, the same photospheric luminosity is predicted, with a similar spectrum that peaks near 1 MeV but has a smaller low-energy slope α . Should the collisional heating turn off in the jet (e.g. as a result of neutron migration or absence of neutrons), a photospheric spectrum with the exponential cutoff near 1 MeV would be produced.

The slope α of photospheric spectrum is limited by the transfer effects discussed in Section 2. The hardest slope found in our radiative transfer models near 10 keV is about 0.4 (for comparison, a Planck spectrum would have $\alpha = 1$). The dominant majority of observed GRBs satisfy this limit (e.g. Preece et al. 2000). However, larger α were reported for a few bursts (Crider et al. 1997; Ghirlanda, Celotti & Ghisellini 2003; Ryde et al. 2006). This suggests that in some bursts the jet can be inhomogeneous on tiny angular scales $\delta\theta < 1/\Gamma$.

The bulk of collisional heating occurs at small radii $r \lesssim R_*$, yet its impact on the plasma and radiation components of the jet is profound and long-lasting. The jet remains forever dominated by e^\pm , $n_\pm \gg n$. The produced radiation remains embedded in the jet until it expands to $r \sim 10^{16}$ cm. Any heating processes between the photosphere and 10^{16} cm occur in the radiation field already changed by the collisional heating.

The collisional heating alone gives a ‘minimal’ emission model that does not include particle acceleration at shocks or other collisionless processes that may occur in the jet. The minimal model provides a natural explanation for observed spectra between ~ 10 keV and \sim GeV. The small radius of this emission is consistent with the strong ms variability observed in many GRBs: the photospheric radiation can vary on observed timescales as short as $\delta t_{\text{obs}} \sim (1+z)R_*/c\Gamma^2 \sim 0.1(1+z)$ ms. However, the small radii also imply two limitations: (i) The optical depth to photon-photon absorption $\tau_{\gamma\gamma}$ is large for photons with energy $E' \sim$ a few MeV in the plasma frame, which corresponds to $E \sim \Gamma E'_{\text{max}} \sim$ GeV in the observer frame. The reported > 10 GeV emission in GRB 080916C (Abdo et al. 2009) must be produced at larger radii, where compactness l (and hence $\tau_{\gamma\gamma}$) is much smaller. (ii) Low-frequency synchrotron radiation is strongly self-absorbed at small radii $r \sim R_*$. Reported observations of prompt optical radiation (Beskin et al. 2009) suggest additional emission from large radii.

At large radii $r \gg R_*$, the jet has a low density and collisional two-body processes are negligible; thus only collisionless heating is possible. Internal shocks and magnetic dissipation are the usual candidates for such heating, which can create an additional component of GRB radiation. Neutron-loaded jets offer another efficient heating mechanism at $r \gg R_*$ that is briefly discussed below.

6.2 Decay of neutrons and collisionless heating at $r \gg R_*$

Neutrons carried by GRB jets eventually decay. Their large Lorentz factor implies a long decay time $\Gamma_n t_\beta$ where $t_\beta \approx 900$ s. The mean radius of β -decay is

$$R_\beta = ct_\beta \Gamma_n \approx 3 \times 10^{15} \left(\frac{\Gamma_n}{100} \right) \text{ cm}. \quad (42)$$

The decay occurring inside the jet has a drag effect on the faster proton component and reduces its Lorentz factor (Rossi, Beloborodov & Rees 2006). In essence, the decay injects relatively slow protons that are picked up by the jet with the relative Lorentz factor $\Gamma_{\text{rel}} = (1/2)(\Gamma/\Gamma_n + \Gamma_n/\Gamma)$. This can be described as inelastic sharing of radial momentum between the fast jet and the decaying slow neutrons, which decelerates and heats the jet. The dissipation efficiency of this process can exceed 100 per cent as the jet tends to use the heat to regain its Lorentz factor via adiabatic cooling and re-dissipate the energy.

Most of neutrons decay near the radius R_β . However, a fraction r/R_β decays at smaller radii $r < R_\beta$. Dissipation of ~ 100 per cent of the jet energy begins at radius $R_1 \sim (\Gamma_n/\Gamma)R_\beta$. Between R_1 and R_β , the jet decelerates in the background of decaying neutrons in a self-similar regime (resembling the deceleration of adiabatic blast waves), and its Lorentz factor decreases as $r^{-1/2}$. This strong dissipation may generate radiation.

Note that the decaying neutrons create a perfect maser. The new protons injected by β -decay appear in the plasma frame with momentum antiparallel to the flow direction and perpendicular to the magnetic field. They immediately begin to gyrate with Lorentz factor Γ_{rel} and form a ring in the momentum space. This ring is a maser that amplifies low-frequency cyclotron waves in the plasma. The maser instability develops on a short timescale proportional to ω_B^{-1} where $\omega_B = eB/m_e c$ (e.g. Hoshino & Arons 1991). Damping of the excited waves heats the plasma. The waves may also accelerate particles. Extremely relativistic ion rings were previously studied near the termination shocks of pulsar winds and proposed to accelerate leptons (Hoshino et al. 1992). A similar heating is observed in the interaction of comets with the solar wind. In this case, a compound flow is formed as the neutral gas around the comet penetrates the solar wind; ionization of the neutral particles effectively injects charges that move with a suprathermal velocity relative to the wind plasma and immediately begin Larmor rotation.

The β -decay and maser instability produce strong volume heating between R_1 and R_β . The jet becomes transparent to very high-energy photons at these radii, and photons with $E > 10$ GeV can be emitted. At comparable radii, optical radiation is released as self-absorption ceases in the optical band. The radiative efficiency is, however, uncertain and likely smaller than the photospheric $\epsilon_* \sim 0.3 - 0.5$. The emission will occur in the optically thin zone and can be of the type modeled by Stern & Poutanen (2004) and more recently by Vurm & Poutanen (2009). The study of possible radiative signatures of neutron decay between R_1 and R_β is deferred to a future paper.

One feature of emission powered by neutron decay can be predicted. The emission will arrive to distant observers with a slight delay with respect to the photospheric emission produced by the same neutrons via the collisional mechanism at $r \lesssim R_*$. As the jet expands from R_* to $r \gg R_*$, a neutron with Lorentz factor Γ_n shifts with respect to the plasma jet a radial distance $\Delta r \approx (r - R_*)(\Gamma_n^{-2} - \Gamma^{-2})/2 \approx$

$r/2\Gamma_n^2$, which corresponds to observed delay

$$\begin{aligned}\Delta t_{\text{obs}} &\approx (1+z) \frac{r}{2\Gamma_n^2 c} \approx \frac{(1+z)t_\beta}{2\Gamma} \left(\frac{r}{R_1} \right) \\ &\approx \frac{(1+z)}{2} \left(\frac{\Gamma}{900} \right)^{-1} \left(\frac{r}{R_1} \right) \text{ s.}\end{aligned}\quad (43)$$

This neutron-drift delay appears to be consistent with the detected delay $\Delta t_{\text{obs}} \sim 2$ s of the prompt optical emission with respect to the main GRB pulses in the ‘naked-eye’ GRB 080319B (Beskin et al. 2009).

REFERENCES

- Abdo A. A. et al., 2009, *Science*, 323, 1688
 Amsler C. et al., *Physics Lett. B* 667, 1 (2008)
 Bahcall J. N., Mészáros P., 2000, *Phys. Rev. Lett.*, 85, 1362
 Band D. L. et al., 2009, *ApJ*, in press (arXiv:0906.0991)
 Beloborodov A. M., 2000, *ApJ*, 539, L25
 Beloborodov A. M., 2003, *ApJ*, 588, 931
 Beskin, G. et al. 2009, submitted to *Science* (arXiv:0905.4431)
 Bosnjak Z., Daigne F., Dubus G. 2009, *A&A*, in press (arXiv:0811.2956)
 Breakstone A. et al., 1984, *Phys. Rev. D*, 30, 528
 Chen W.-X., Beloborodov A. M., 2006, *ApJ*, 657, 383
 Crider A. et al., 1997, *ApJ*, 479, L39
 Derishev E. V., Kocharovskiy V. V., Kocharovskiy V. V., 1999, *ApJ*, 521, 640
 Fukuda S. et al., 2002, *ApJ*, 578, 317
 Fuller G. M., Pruet J., Abazajian K., 2000, *Phys. Rev. Lett.*, 85, 2673
 Ghisellini G., Celotti A., 1999, *ApJ*, 511, L93
 Ghirlanda G., Celotti A., Ghisellini G., 2003, *A&A*, 406, 879
 Giannios D., Spruit H. C., 2007, *A&A*, 469, 1
 Hoshino M., Arons J., 1991, *Phys. Fluids*, B, 3, 818
 Hoshino M., Arons J., Gallant Y. A., Langdon A. B., 1992, *ApJ*, 390, 454
 Lemoine M., 2002, *A&A*, 390, L31
 Lightman A. P., Zdziarski A., 1987, *ApJ*, 319, 643
 Mészáros P., Rees M. J., 2000, *ApJ*, 541, L5
 Metzger B. D., Thompson T. A., Quataert, E., 2008, *ApJ*, 676, 1130
 Paczyński B., 1990, *ApJ*, 363, 218
 Pe’er A., Mészáros P., Rees M. J., 2005, *ApJ*, 635, 476
 Piran T., 2005, *Rev. Mod. Phys.*, 76, 1143
 Preece R. D. et al., 2002, *ApJS*, 126, 19
 Pruet J., Woosley S. E., Hoffman R. D., 2003, *ApJ*, 586, 1254
 Rees M. J., Mészáros P., 2005, *ApJ*, 628, 847
 Rossi E. M., Beloborodov A. M., Rees M. J., 2006, *MNRAS*, 369, 1797
 Ryde F., Svensson, R., 1999, *ApJ*, 512, 693
 Ryde F. et al., 2006, *ApJ*, 652, 1400
 Sironi L., Spitkovsky A., 2009, *ApJ*, 698, 1523
 Spitzer L., 1956, *Physics of Fully Ionized Gases* (New York: Interscience)
 Stern B. E., Poutanen J., 2004, *MNRAS*, 352, 35
 Svensson R., 1987, *MNRAS*, 227, 403
 Thompson C., 1994, *MNRAS*, 270, 480
 Vurm I., Poutanen J., 2009, *ApJ*, 698, 293

APPENDIX A: ELECTRON-POSITRON CASCADE

The compactness parameter l is large in the region of collisional heating (Section 4.2). It implies the quick Compton cooling and the quick γ - γ reaction for photons above the threshold for e^\pm pair creation. Therefore, the timescale for the cascade development following the injection of an electron (or positron) with $\gamma_0 \sim m_\pi/m_e$ is short compared with the jet expansion timescale. Then the distribution function of nonthermal e^\pm , $dn_\pm/d\gamma$, is locally (at a given r) quasi-steady and satisfies the equation

$$\frac{d}{d\gamma} \left(\frac{dn_\pm}{d\gamma} \dot{\gamma} \right) = S(\gamma), \quad (A1)$$

where $S(\gamma) = d\dot{n}_\pm/d\gamma$ is the creation rate of secondary e^\pm , and $m_e c^2 \dot{\gamma}(\gamma)$ is the energy loss rate of electron (or positron) with a Lorentz factor γ . The energy loss is due to Compton scattering, synchrotron emission, and Coulomb collisions with thermal electrons and positrons.¹¹ Coulomb collisions dominate at small $\gamma \approx 1$ (and lead to quick thermalization of nonrelativistic e^\pm). In this Appendix, we focus on the relativistic tail of the e^\pm distribution, where Coulomb collisions are negligible compared with Compton and synchrotron losses. Then,

$$m_e c^2 \dot{\gamma} \approx -\frac{4}{3} \sigma_{\text{T}} c (U_{\text{KN}} + U_B)(\gamma^2 - 1), \quad (A2)$$

where $U_{\text{KN}}(\gamma)$ is the energy density of photons with energy $E' \lesssim m_e c^2/\gamma$, i.e. below the Klein-Nishina cutoff in the scattering cross section.

The source function $S(\gamma)$ may be written as

$$S(\gamma) = g(\gamma) \mathcal{M}_0 \dot{n}, \quad \mathcal{M}_0 = \frac{f_\pm \Gamma_{\text{rel}} m_p}{\gamma_0 m_e}. \quad (A3)$$

Here \dot{n} is the rate of nuclear collisions in the compound flow (eq. 7), and \mathcal{M}_0 is the multiplicity of primary e^\pm injected with Lorentz factor γ_0 following a nuclear collision. Then $g(\gamma)$ is a dimensionless function that represents the source of secondary e^\pm created by one primary e^- or e^+ . This function is calculated numerically using Monte-Carlo simulations of the cascade.

Integration of equation (A1) yields

$$\frac{d\tau_{\text{nth}}}{d\gamma} \equiv \frac{\sigma_{\text{T}} r}{\Gamma} \frac{dn_\pm}{d\gamma} = \frac{3}{8} \mathcal{M}_0 \tau_n \frac{nm_e c^2}{U_{\text{KN}} + U_B} \frac{G(\gamma)}{\gamma^2 - 1}, \quad (A4)$$

$$G(\gamma) \equiv \int_\gamma^{\gamma_0} g(\gamma') d\gamma'. \quad (A5)$$

When $U_B \ll U_\gamma$, this equation becomes

$$\frac{\sigma_{\text{T}} r}{\Gamma} \frac{dn_\pm}{d\gamma} = \frac{3}{8} \mathcal{M}_0 \tau_n \frac{n}{n_\gamma} \frac{G(\gamma)}{\bar{\varepsilon}(\gamma)(\gamma^2 - 1)}, \quad (A6)$$

where $n_\gamma/n \sim 10^5$ is the photon-to-baryon ratio (the main parameter of the GRB jet, see eq. 2), and $\bar{\varepsilon}(\gamma) \equiv U_{\text{KN}}/n_\gamma m_e c^2$ represents the mean dimensionless energy per photon below the Klein-Nishina cutoff. The typical $\bar{\varepsilon}$ in the calculated models is near 3×10^{-3} and varies slowly with γ .

¹¹ We neglect in this paper the possibility of energy exchange between thermal plasma and nonthermal e^\pm due to collective processes.

The dimensionless function $G(\gamma)$ equals the number of secondary e^\pm injected with Lorentz factor above a given γ in the e^\pm cascade triggered by one primary particle. In particular, $G(1) = \mathcal{M}_s$ is the total number of secondary e^\pm . The function $G(\gamma)$ decreases from $G(1) = \mathcal{M}_s$ to $G(\gamma) \sim 1$ at $\gamma \lesssim \gamma_0$, which implies a relatively slow dependence on γ , with the average slope $d \ln G / d \ln \gamma \approx -\ln \mathcal{M}_s / \ln \gamma_0 \approx -0.7$. Then equation (A6) implies that the optical depth of the nonthermal e^\pm population τ_{nth} sharply peaks at $\gamma \sim 1$. Its value is small, $\tau_{\text{nth}} \ll 1$ (and much smaller than the optical depth of the thermalized e^\pm). However, the effect of nonthermal population on radiation is measured not by τ_{nth} , but by the Compton amplification factor $A = \int \gamma^2 d\tau_{\text{nth}}$. The amplification factor peaks at large γ ,

$$\frac{dA}{d \ln \gamma} = \frac{3m_e}{8m_p} \mathcal{M}_0 \tau_n \frac{n}{n_\gamma} \frac{\gamma G(\gamma)}{\bar{\varepsilon}(\gamma)}, \quad (\text{A7})$$

Particles with $\gamma^2 \bar{\varepsilon} \gg 1$ generate photons that are absorbed by the $\gamma - \gamma$ reaction. As a result, particles with $\gamma \gtrsim 20$ contribute mainly to the development of the e^\pm cascade, while particles with $\gamma \lesssim 20$ shape the scattered radiation spectrum.

APPENDIX B: NUMERICAL CODE

The code is designed to simulate the self-consistent evolution of the radiation field and the e^\pm plasma in the jet. For collisionally heated jets considered in this paper, the following quantities are known at all radii: the injection rate of primary e^\pm with $\gamma_0 \sim 300$ (eq. 7) and the corresponding energy injection rate (eq. 9), the density of the accumulated thermalized e^\pm component (eq. 24) and the heating rate of this component (eq. 29). The code aims to find the temperature of the thermalized e^\pm population $T_e(r)$, the nonthermal tail of e^\pm distribution, and the radiation field at all radii.

The calculation is split into two parts: (A) global radiative transfer in a jet with a given e^\pm distribution, and (B) calculation of $T_e(r)$ and the nonthermal tail of e^\pm distribution for a given radiation field. The consistency between parts A and B is reached via iterations as explained below. Note that part A is a global problem, while part B is local and can be solved separately at all radii, because T_e and the e^\pm tail at a given r are determined by the *local* radiation field, heating rate, and e^\pm injection rate.

The radiation has a Planck spectrum at early stages of jet expansion (i.e. at small radii), with the temperature determined by the initial size of the jet and its energy. In the simulations, the initial thermal radiation is sampled by a large number of Planck photons ($\sim 10^7$), which are injected at a small radius and their scattering is followed until the photons escape. The code can also simulate the injection of synchrotron photons and follow them together with the Planck photons. Before the jet expands to transparency, the photons are multiply scattered and may be absorbed by the $\gamma - \gamma$ reaction. In each scattering event, the scattering electron is randomly drawn from the local e^\pm population, and the exact Compton cross section is used to randomly perform the scattering.

The transfer is calculated in the static lab frame, assuming that the plasma flows in the radial direction with a bulk Lorentz factor Γ . Since Γ is large ($10^2 - 10^3$ in the

simulations) essentially all photons flow outward, and most of them have tiny angles $\theta \sim \Gamma^{-1}$ with respect to the radial direction. The radiation is essentially comoving with the plasma flow. Therefore, one can view the transfer as the evolution of radiation in time $t = r/c$ — time and radius are almost equivalent choices for the independent variable in the problem. Between successive scatterings at radii r_1 and r_2 , the photon propagates along a straight line in the lab frame, and its angle with respect to the local direction of the radial jet, θ , changes: $\sin \theta_2 = (r_1/r_2) \sin \theta_1$. This change automatically (and exactly) describes the adiabatic cooling of radiation in the opaque zone.¹²

When solving the radiative transfer with a trial $T_e(r)$, we find the energy gained by radiation (per photon) from scattering on thermal e^\pm . This is done by defining a radial grid r_i and accumulating statistics of scattering in each bin $\Delta \ln r$ during the Monte-Carlo simulation of the radiative transfer. Thus, we evaluate $(d\bar{E}/d \ln r)_{\text{th}}(r)$ for our trial model. If it exceeds the required $(d\bar{E}/d \ln r)_{\text{th}}$ (given in eq. 40) we reduce $T_e(r)$ in the next iteration.

The nonthermal tail is given by equation (A4), which contains the cascade function $G(\gamma)$. We find $G(\gamma)$ numerically using the Monte-Carlo simulation of the cascade in the local radiation field (which is known after calculating the radiative transfer in the previous iteration). The updated nonthermal tail and T_e are used in the calculation of radiative transfer in the next iteration. 5-10 iterations are usually sufficient to accurately find the self-consistent solution for the radiative transfer and e^\pm distribution.

A faster approximate method of modeling the nonthermal tail assumes a fixed shape of the cascade function $G(\gamma)$ at all radii. Then the e^\pm distribution function in the tail may be written in the form $f_{\text{nth}}(\gamma, r) = K(r)h(\gamma)$, where $h(\gamma)$ is a fixed function normalized to unity and $K(r)$ is the amplitude of the tail, which depends on radius. The function $h(\gamma)$ is proportional to $G(\gamma)/\bar{\varepsilon}(\gamma)\gamma^2$ (cf. eq. A6). For saturated cascades with a fixed injection Lorentz factor γ_0 , $h(\gamma)$ weakly depends on the details of the target radiation spectrum. It can be calculated once for a typical radiation spectrum — a power law with photon index $\beta = 2$ and a low-energy cutoff at $2.7kT(R_n)$. In this approximation, one needs to iterate only the normalization factor $K(r)$. The iterations are done similarly to the iterations of T_e : when solving the radiative transfer with a trial $K(r)$, we find the energy gained by radiation (per photon) from scattering on the nonthermal tail. If it exceeds the required $(d\bar{E}/d \ln r)_{\text{nth}}$ (given in eq. 41) we reduce $K(r)$ in the next iteration.

¹² This can be understood by considering the toy problem of coherent and isotropic scattering in a cold jet. Then a scattering event does not change the photon energy in the local plasma frame E' ; it only changes its angle. Between successive scatterings, the energy of the freely propagating photon in the lab frame $E = \text{const}$, and $E' = E\Gamma(1 - \beta \cos \theta)$ is decreasing because of decreasing θ . In addition, the propagating photon becomes preferentially beamed outward in the plasma frame (θ' decreases). Next scattering again randomizes $\cos \theta'$ and destroys the preferential beaming, suddenly increasing (on average) θ' . As a result, the next scattering on average reduces the photon energy $E = E'\Gamma(1 + \beta \cos \theta')$ in the lab frame.